Geoscientific
Instrumentation
Methods and
Data Systems

New proglacial meteorology and river stage observations from Inglefield Land and Pituffik, NW Greenland

Sarah E. Esenther[1,2], **Laurence C. Smith**[1,2], **Adam LeWinter**[3], **Lincoln H. Pitcher**[4,5], **Brandon T. Overstreet**[6], **Aaron Kehl**[3], **Cuyler Onclin**[7], **Seth Goldstein**[2], and **Jonathan C. Ryan**[8]

[1]Department of Earth, Environmental, and Planetary Sciences (DEEPS), Brown University, Providence, RI 02912, USA
[2]Institute at Brown for Environment and Society (IBES), Brown University, Providence, RI 02912, USA
[3]U.S. Army Corps of Engineers, Cold Regions Research and Engineering Laboratory, Hanover, NH 03755, USA
[4]Cooperative Institute for Research in Environmental Sciences (CIRES),
University of Colorado (CU) Boulder, Boulder, CO 80309, USA
[5]Oak Ridge Institute for Science and Education (ORISE), Oak Ridge, TN 37830, USA
[6]Department of Geology and Geophysics, University of Wyoming, 1000 E. University Avenue, Laramie, WY 82071, USA
[7]independent researcher: Saskatoon, SK S7J2S1, Canada
[8]Department of Geography, University of Oregon, Eugene, OR 97401, USA

Correspondence: Sarah E. Esenther (sarah_esenther@brown.edu)

Abstract. Meltwater runoff from the Greenland ice sheet (GrIS) is an important contributor to global sea level rise, but substantial uncertainty exists in its measurement and prediction. Common approaches for estimating ice sheet runoff are in situ gauging of proglacial rivers draining the ice sheet and surface mass balance (SMB) modeling. To obtain hydrological and meteorological data sets suitable for both runoff stage characterization and, pending the establishment of stage–discharge curves, SMB model evaluation, we established an automated weather station (AWS) and a cluster of traditional and experimental river stage sensors on the Minturn River, the largest proglacial river draining Inglefield Land, NW Greenland. Secondary installations measuring river stage were installed in the Fox Canyon River and North River at Pituffik Space Base, NW Greenland. Proglacial runoff at these sites is dominated by supraglacial processes only, uniquely advantaging them for SMB studies. The three installations provide rare hydrological time series and an opportunity to evaluate experimental measurements of river stage from a harsh, little-studied polar region. The installed instruments include submerged vented and non-vented pressure transducers, a bubbler sensor, experimental bank-mounted laser rangefinders, and time-lapse cameras. The first 3 years of observations (2019 to 2021) from these stations indicate (a) a meltwater runoff season from late June to late August/early September that is roughly synchronous throughout the region; (b) the early onset ($\sim$ 23 June to 8 July) of a strong diurnal runoff signal in 2019 and 2020, suggesting minimal meltwater storage in snow and/or firn; (c) 1 d lagged air temperature that displays the strongest correlation with river stage; (d) river stage that correlates more strongly with ablation zone albedo than with net radiation; and (e) the late-summer rain-on-ice events appear to trigger the region's sharpest and largest floods. The new gauging stations provide valuable in situ hydrological observations that are freely available through the PROMICE network (https://promice.org/weather-stations/, last access: 14 September 2023).

1 Introduction

Besides solid ice discharge, climate-change-induced meltwater runoff is a dominant driver of the Greenland ice sheet (GrIS) mass loss (Mottram et al., 2019; Mouginot et al., 2019; Shepherd et al., 2020; King et al., 2020) that is projected to increase throughout the 21st century (Trusel et al., 2018; Noël et al., 2021; Hofer et al., 2020). However, current

climate models typically calculate runoff as a residual term in surface mass balance budgets (van Dalum et al., 2021). As runoff represents rain and meltwater that is not refrozen or retained in the firn, errors in the surface energy balance terms used to calculate melt and/or refreezing, or in any of the other surface mass balance terms, propagate to errors in the subsequent runoff term calculation. There is therefore a growing need for accurate, in situ hydrological data sets for characterizing runoff magnitude and timing, as well as evaluating ice sheet surface mass balance (SMB) models (Smith et al., 2017, 2021). In situ measurements of runoff are useful for direct observation of GrIS runoff contributions to sea level rise, as well as for assessing hydrological models, hydropower potential, and freshwater resources critical for decision-makers (Smith et al., 2017; Alther et al., 1981; Instanes et al., 2015).

Despite this need for in situ hydrological measurements, only a small handful of GrIS proglacial rivers have been gauged outside of SW Greenland (Ploeg et al., 2021; Mankoff et al., 2020; Mernild et al., 2008), and the majority of modeled runoff evaluation studies have been conducted in SW Greenland (Smith et al., 2017; Mernild et al., 2011, 2018; Cooper et al., 2018; Smith et al., 2015). The NW GrIS has also experienced extensive melting since 2000 and is now one of the largest contributors to GrIS mass losses (Mouginot et al., 2019). By 2100, runoff mass losses from the NW GrIS are projected to reach $201\,\mathrm{Gt\,yr^{-1}}$, far exceeding the anticipated dynamic losses of $22\,\mathrm{Gt\,yr^{-1}}$ from the region at that time (Muntjewerf et al., 2020). However, the NW GrIS lacks in situ measurements necessary to characterize the region's hydrometeorology, quantify runoff drainage to the ocean, and evaluate SMB models.

More generally, permanent river gauging installations are time- and resource-intensive to install and maintain in remote, harsh Arctic environments. Proglacial river gauging sites are typically difficult to maintain due to high-sediment bedload and shifting braided channels. In situ sensor systems generally require expert installation and repair, a difficulty compounded in remote study locations with poor accessibility. Traditional pressure-based river gauge technologies (i.e., pressure transducers or PTs) require full immersion and are thus poorly suited for Arctic rivers in which thick ice, spring floods, and rolling cobbles can cause sensor damage, movement, or loss. Recently, non-contact methods of river stage measurement, including radar, laser rangefinder, and camera, have received increasing interest (Bandini et al., 2022; Paul et al., 2020; Goldstein et al., 2023), but laser rangefinder and radar sensors are traditionally nadir-looking and thus require mounting to a bridge, precluding their use in undeveloped Arctic locations. To our knowledge, no in situ hydrological observations of this length (3+ years) are currently available for NW Greenland, an exceedingly cold and remote region.

Analysis of runoff stage data enables the evaluation of diurnal, seasonal, and annual runoff patterns, as well as the assessment of the relationship between these patterns and me-

teorological drivers. However, as SMB climate models estimate runoff flux, river stage measurements alone cannot be directly compared with SMB outputs. River stage measurements must be combined with a stage–discharge curve (established with in situ discharge measurements) and careful watershed delineation to allow for comparison between in situ runoff flux and SMB climate model runoff flux. Such discharge measurements were recently collected by the author team and are currently undergoing quality control measures. These data will be presented with a remotely sensed ice watershed delineation and SMB model outputs in a future publication.

This paper describes new hydrometric sensor installations and the resulting 3-year time series (2019–2021) of the river stage (water level) at three proglacial gauging sites in NW Greenland. The sensors include vented and non-vented PTs, a bubbler sensor, bank-mounted laser rangefinders, and time-lapse cameras to record the river stage (water level) and an automated weather station (AWS). The bank-mounted laser rangefinders are oblique-looking, which is a novel approach to the laser rangefinder stage measurement for remote river gauges. An initial assessment of the data and instrument performance is provided for the 2019–2021 runoff seasons. To mitigate intermittent data gaps found in all instruments, we also create a hybrid, multisensor river stage product for the Minturn River, Inglefield Land. Following technical descriptions of the instruments and performance, a preliminary characterization of diurnal, seasonal, and interannual variability in NW GrIS meltwater runoff is presented. We conclude that experimental new hydrometeorological sensor installations can improve our physical understanding of ice sheet runoff and SMB for a remote, little-studied, and hydrologically active area of the GrIS.

2   Study sites

In July 2019, we established three new hydrometric sensor installations on the Minturn River (78.590801°, −68.992706°; Inglefield Land), North River (76.538980°, −68.728190°; located at Pituffik Space Base or SB), and Fox Canyon River (76.466460°, −68.579060°; near Pituffik SB; Fig. 1). The Minturn River watershed is the largest of the three ($\sim 3800\,\mathrm{km^2}$; $\sim 75\,\%$ glaciated) with elevations ranging from 314 to 1653 m (Fig. 1a). Due to differences between digital elevation model (DEM)-based watershed delineations of the Minturn, the estimate of $\sim 3800\,\mathrm{km^2}$ is an acceptable approximation for this paper. The smaller North River ($229\,\mathrm{km^2}$; $\sim 56\,\%$ glaciated) and Fox Canyon River ($115\,\mathrm{km^2}$; $\sim 31\,\%$ glaciated) watersheds drain through or near Pituffik SB (Fig. 1b and c), with elevations ranging from 59–1045 m to 199–913 m, respectively. In each of the watersheds, the ice sheet is fully grounded, with no known surface-to-bed connections (i.e., moulins or water-filled crevasses). Instead, ice sheet runoff is routed entirely over the ice sur-
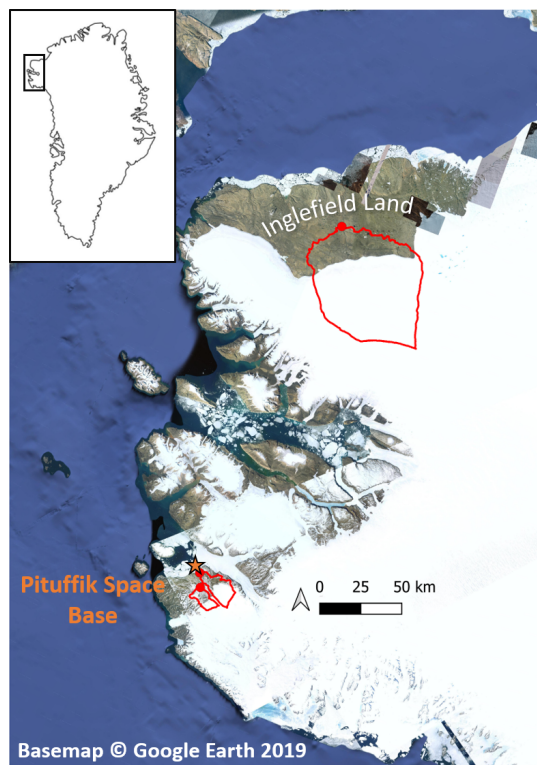
Figure 1. New river stage measurements are available for the following three glacial/proglacial watersheds in NW Greenland: **(a)** Minturn River, **(b)** North River, and **(c)** Fox Canyon River. Instrument installations were established at ($78.590801°$, $-68.992706°$), ($76.538980°$, $-68.728190°$), and ($76.466460°$, $-68.579060°$), respectively, in July 2019 (red dots). The most comprehensive suite of sensors, including an automated weather station (AWS), is installed at the Minturn River, Inglefield Land **(a)**. Pituffik Space Base, which collects airport meteorological records, is indicated by the star. The basemap is credited to © Google Earth 2019.

Figure 2. GrIS runoff in Inglefield Land is routed entirely over the ice sheet surface through long, semi-parallel supraglacial streams directly onto the bedrock-dominated proglacial zone, making it an ideal location to study surface runoff without interference from en- or sub-glacial processes. The absence of bedload and suspended sediment in the Minturn River at the ice margin further affirms the primacy of supraglacial runoff at this site (photo credit: Laurence C. Smith).

face through long, semi-parallel supraglacial streams directly onto bedrock-dominated proglacial zones (Fig. 2; see also Yang et al., 2019; Li et al., 2022), signifying that proglacial runoff is dominated by surface processes with negligible influence of en- or sub-glacial hydrology. The dominance of supraglacial hydrology in NW Greenland is distinctly different from the SW GrIS, where surface runoff typically enters moulins prior to reaching the proglacial zone (Smith et al., 2015; Yang and Smith, 2016), sometimes even at high elevations (Gagliardini and Werder, 2018).

3 Instruments and data collection

3.1 Minturn River, Inglefield Land

The hydrometric sensor package at the Minturn River includes a compact constant flow bubbler; two custom-built, bank-mounted, and oblique-looking laser rangefinder

systems; an AWS; and two StarDot NetCam SC 5 MP (megapixel) cameras. The bubbler, which began measurement on 9 July 2019, is a Sutron® Constant Flow bubbler (CF bubbler; Compact Constant Flow Bubbler, 2022), a self-contained, precision device to measure water level and temperature. The CF bubbler consists of a pump, tank, manifold, control board, display/keypad within a $26.7\,\mathrm{cm} \times 21.6\,\mathrm{cm} \times 19.0\,\mathrm{cm}$ polycarbonate NEMA 4X enclosure. Measurements are collected every 15 min and transmitted via an Iridium satellite modem every hour. In 2021, an additional vented Level TROLL 700H data logger pressure transducer (PT) was installed at the site. The sensor is contained in a titanium body and measures water pressure and temperature, from which water level is determined. This second vented Level TROLL PT has operated across the river channel from the CF bubbler since 16 June 2021.

River stage measurements are complemented by two custom-built, bank-mounted, and oblique-looking laser rangefinder systems, M1 and M2 (one on each riverbank; Fig. 3). These ruggedized systems were built at the Cold Regions Research and Engineering Laboratory (CRREL) in collaboration with Crane Johnson from the National Weather Service, who previously developed their concept and programming. A Laser Technology, Inc. (LTI), TruSense S200 (Buytaert and Sah, 2020) sensor, which is a time-of-flight-based, long-range distance finder utilizing the 905 nm wavelength, and an inclinometer are contained in an aluminum enclosure positioned with a clear line of sight to the water surface. A total of 50 laser returns are recorded on the hour, each hour, and recorded by a Campbell Scientific CR1000X data logger, along with battery voltage, panel temperature, and inclinometer angle. Hourly first, strongest, and last laser returns are transmitted with the system information, and the

number of transmission tries are provided via the Iridium satellite network. The system is powered by a 10 W solar panel on a versatile polar mast mounting system, with energy stored in a deep-cycle sealed lead acid battery.

Meteorological measurements are collected by an AWS which was installed at the Minturn River on 9 July 2019 (Fig. 4). Wind speed and direction are measured with a Sutron ultrasonic wind sensor 5600-0215 (Wind Speed, 2022). Two Kipp & Zonen CMP3 pyranometers (Kipp and Zonen, 2022), with one facing upward and one facing downward, measure incoming and reflected solar irradiance. A Sutron Accubar barometric pressure sensor 5600-0120 (Accubar, 2022) is used, and it contains a highly accurate solid-state pressure transducer that measures barometric pressure. Air temperature is recorded to the nearest $\pm 0.1\,°C$ by a Sutron air temperature sensor 5600-0020 (Air Temperature, 2022) and to the nearest $\pm 0.3\,°C$ by a Sutron AT/RH (ambient temperature and relative humidity) high-accuracy sensor (AT/RH, 2022), which additionally measures relative humidity to the nearest $\pm 1.5\,\%$. These AWS measurements are collected every 15 min and telemetered via Iridium satellite modem every hour.

Finally, two StarDot NetCam SC 5 MP cameras (Multi-Megapixel, 2019), which were installed on 12 July 2019, collect images of the Minturn River and foreground every 3 h when there is sufficient ambient lighting (e.g., nighttime and winter images will be underexposed and are therefore not useful data). The timing of these image acquisitions is alternated, yielding an image every 1.5 h. Images are transmitted to CRREL via the Iridium satellite modem. Each camera view includes the opposite bank of the river, allowing for calculation of river stage through edge detection (Goldstein et al., 2023), and visual evidence of river ice, rain, snow, and other environmental conditions.

During the July 2019 field campaign, terrestrial laser scanner (TLS) elevation point clouds of the site were collected with a RIEGL VZ-400i 3D laser scanner (RIEGL, 2023), using a Trimble R10 base station and rover for global navigation satellite system (GNSS) positional measurements. Scans were taken from 27 positions around the site between 10 and 11 July 2019. Scans from each position were aggregated into a 3D digital elevation model (DEM) that includes all permanently installed instrumentation. Optical surveys were conducted from 8 to 11 July 2019 to independently establish the elevations of instruments and river stage relative to newly established benchmarks.

Annual service trips have been completed since the instrument cluster was established in 2019. Due to international research travel restrictions to Greenland during the COVID-19 pandemic, Asiaq (Greenland Survey) and Vectrus (a mission-support organization servicing Pituffik SB; https://gov2x.com/, last access: 14 September 2023) completed the 2020 and 2021 service trips, respectively. The Asiaq service trip on 21 June 2020 replaced the AWS batteries, corrected the wiring of its solar panel, replaced its

Figure 3. Bank-mounted, oblique-looking laser rangefinder recording the river stage on the right bank of the North River, Pituffik SB. In total, four identical laser rangefinder units were built and installed in NW Greenland, with two at the Minturn River (Inglefield Land), one at the North River (Pituffik SB), and one at Fox Canyon River (Pituffik SB). The single-shot laser rangefinder measures distance between the sensor and water surface using the time of flight of the emitted and reflected beam. This novel approach to river stage measurement avoids contact with water, thus reducing the risk of sensor damage or loss from ice, rolling cobbles, and spring breakup floods (photo credit: Lincoln Pitcher).

SD card, replaced a SIM card for the right bank time-lapse camera, power-cycled the lasers, and repaired a broken wire on the Sutron CF bubbler. During a subsequent Vectrus service trip on 12 June 2021, data were manually downloaded from all stations, the laser unit software was updated to retain the date while in sleep mode and wake up automatically on April 1, the batteries and charge controllers were all checked, the Level TROLL pressure transducer was installed, and all stations that had not yet turned on for the year were power-cycled.

Figure 4. Automated weather station and CF bubbler with a vented pressure transducer (on the left) and a time-lapse camera (on the right) established at the Minturn River. Other instruments at this site include two bank-mounted laser rangefinders, a second vented pressure transducer, and a second time-lapse camera on the opposite bank (photo credit: Lincoln Pitcher).

3.2 North and Fox Canyon River, Pituffik SB

On the right bank of the North River, a third custom-built, bank-mounted LTI TruSense S200 laser rangefinder ranging system, N1, was installed during July 2019 and programmed to retrieve and telemeter river stage estimates every hour. As before, telemetry is achieved via an Iridium satellite modem. Two Solinst Levelogger instruments (non-vented, self-contained, and self-logging PTs) were installed on the left bank of the North River in July 2019 to record the stage, with one inserted on a slotted steel pipe and the other inserted in a slotted PVC pipe. A single corresponding Solinst Barologger was placed in the bank-mounted laser rangefinder box to record the atmospheric pressure variations for the later correction of the two PT stage records. All three pressure transducers record data every 15 min, which is aligned with the single-beam laser rangefinder. Due to the close alignment of the two non-transmitting Levelogger records, the more complete Levelogger record was identified as the preferred pressure transducer record for the North River during the time period from 17 July 2019 to 22 May 2021.

A vented Level TROLL 700H data logger PT was installed alongside the laser rangefinder on the North River in 2021 and began transmitting records on 4 June 2021. This vented Level TROLL PT is used as the PT stage record beginning on 4 June 2021. These measurements were complemented by TLS elevation point clouds of the North River, which were acquired on 5 July 2019 from 12 positions with the RIEGL VZ-2000 3D laser scanner, Trimble R10 base station, and rover for GNSS positional measurements. Scans from three additional positions were performed on 5 and 9 October 2019. Optical surveys were conducted between 30 June and 5 July 2019, tying the water level measurements to three newly established fixed benchmarks on boulders along the bank.

A Vectrus service trip on 12 June 2021 downloaded the data files, power-cycled the laser, checked the batteries and charge controllers, updated the laser software to allow for automatic spring wake-up, and installed the vented PT.

At the Fox Canyon River, a fourth custom-built, bank-mounted LT TruSense S200 laser rangefinder ranging system, F1, was installed on 15 July 2019 and programmed to retrieve river stage measurements every 15 min and telemeter them hourly via an Iridium satellite modem. A RIEGL VZ-2000 3D laser scanner survey was performed during this initial installation trip to establish benchmarks. Optical surveys at the Fox Canyon River Bridge were performed between 1 and 4 July 2019, using the three newly established fixed benchmarks. On 12 June 2021, a Vectrus service visit downloaded the data files, power-cycled the laser, checked the batteries and charge controllers, and updated the laser software for spring wake-up.

3.3 Data telemetry, downloads, and public release

Data from all four bank-mounted laser rangefinder systems, the Minturn River CF bubbler, the Minturn and North rivers Level TROLL PTs, the Minturn River time-lapse cameras, and the Minturn River AWS are telemetered hourly via the Iridium short-burst data (SBD) network and received by the U.S. Army Corps of Engineers (Esenther et al., 2023). River stage and AWS measurements from the Minturn River are automatically forwarded to the Geological Survey of Denmark and Greenland (GEUS) PROMICE database (https://dataverse.geus.dk/dataverse/PROMICE, last access: 14 September 2023) and included on their website under the station name ING_1 (PROMICE, 2023).

Non-telemetered PTs were downloaded in the field. The North River Levelogger and Barologger PTs were installed on 17 July 2019 and recorded data until 22 May 2021. Minturn River cameras began collecting data on 12 July 2019.

3.4 Remote sensing data

Precipitation, snow cover, and albedo were obtained using satellite sensing to characterize the ice surface conditions for the GrIS ablation zone over each watershed. Due to the small size of the North River and Fox Canyon River watersheds relative to the spatial resolutions of the remote sensing data sets, these data sets are less representative of conditions within the watersheds, and statistical analyses over these watersheds are omitted from this paper. Daily accumulated precipitation was derived from combined microwave infrared (IR) obtained from the Integrated Multi-satellitE Retrievals for Global Precipitation Measurement (IMERG; GPM, 2019). Snow cover data over the three watersheds was obtained from the NDSI_Snow_ Cover layer and albedo was obtained from the Snow_Albedo_Daily_Tile layer in the MODIS/Terra Snow Cover Daily L3 Global 500 m SIN Grid

product, Version 6.1 (data set ID MOD10A1; MODIS, 2023). These remotely sensed precipitation, snow cover, and albedo data products provide insight into additional aspects of the hydrometeorology of Minturn watershed.

3.5 Data processing

Some minor filtering was required to remove anomalous data and outliers. Stage values from the CF bubbler data were clipped to fall between 0.6 m, the lowest value the CF bubbler could read based on its position in the river, and 6 m, a conservative upper estimate of the river stage. At the end of the 2020 melt season (2 to 12 September 2020), the CF bubbler returned some anomalously high stage measurements, likely due to freezing, which were also removed. The CF bubbler pipe was abruptly displaced downward by 0.5 m between 03:15 and 03:30 LT on 29 July 2021, due to turbulent flow, as confirmed by the time-lapse camera imagery. Stage records following the offset were adjusted by +0.5 m to maintain consistency with the rest of the record. This CF bubbler record, along with records from all other stage instruments, was converted to water surface elevation (WSE; WGS 84/UTM zone 19N; ellipsoid height) using optical surveys tied to fixed benchmarks.

Non-telemetered PT data at the North River were downloaded in the field using a Solinst Levelogger optical reader. The two Levelogger PT records were compensated for air pressure using the Barologger PT record and Levelogger 4.6.2 software. As the two Levelogger records were virtually identical, the one with the more complete record is used in the following analysis. Telemetered Level TROLL PT data are compensated for air pressure by CRREL. For analysis, this Level TROLL PT record was converted to WSE, following the methodology described for the CF bubbler (WGS 84/UTM zone 19N; ellipsoid height).

Telemetered returns from the bank-mounted laser rangefinder systems were received and processed into distance values by CRREL. First, last, and strongest values were transmitted to a web page for instantaneous access. To filter outliers present in the Minturn River records, only physically realistic values were retained (between 6 and 20 m for laser rangefinder M1 and between 5 and 15 m for laser rangefinder M2). The median return of each record was then taken as the distance from the laser device to the water surface.

This median laser return distance was then used to calculate the river stage as follows. As all rivers experienced zero flow during the cold season, the median-corrected laser rangefinder return from each record was taken as the distance to the empty riverbed and/or frozen river ice surface, as measured on a zero-flow day. At the Minturn River, zero flow was visually confirmed with camera image records. Simple trigonometry was used to compute the vertical distance of the water surface below the laser box ($Z_{\mathrm{Lidar\,Box}}$), using the measured distance to the water surface (median lidar distance)

and the vertical angle of the laser range finder ($\theta_{\mathrm{Lidar\,Box}}$). This vertical distance was then used to calculate the river stage (Eq. 1) relative to an arbitrary datum, as follows:

$$\mathrm{Stage} = Z_{\mathrm{Lidar\,Box}} - \mathrm{median\ lidar\ distance} \times \sin(\theta_{\mathrm{Lidar\,Box}}). \quad (1)$$

Using the TLS point cloud captured at each study location in 2019, the ellipsoid-referenced elevation of each bank-mounted laser rangefinder unit could be found in the scans, yielding the WSE of each bank-mounted laser rangefinder record (WGS 84/UTM zone 19N). Some fixed anomalous offsets, likely from solar interference, occurred occasionally in some returns, and their correction is described in Appendix A. While the snow depth instrument from the AWS failed to function, all other meteorological instruments functioned as expected, and their records were transmitted to the PROMICE database without further processing.

River stage fluctuations were also extracted from time-lapse camera images by identifying the wetted shoreline position and combining this with the TLS scan of the bank topography (Goldstein et al., 2023). Full details of this method can be found in Goldstein et al. (2023), but, briefly, a Canny edge detector was used to automatically detect the shoreline position from each camera image, with manual delineations performed if necessary. Georectifying these shoreline positions and projecting them onto the TLS scan of the riverbank yielded estimates of river height fluctuation, with an estimated error of ±0.185 m (Goldstein et al., 2023). This camera record has recognized the uncertainty for the lowest ∼75 % of the Minturn River stage values, due to the mathematical extrapolation of the TLS bank scan below the waterline. For our analysis, this camera record was converted to approximate WSE by arbitrarily assigning the WSE of the CF bubbler record to the camera record on a day of zero flow.

Because all sensors experienced occasional data gaps, a hybrid stage product for the Minturn River was created to infill missing data (Fig. 5). Laser rangefinders M1, M2 (Minturn River), N1 (North River), and F1 (Fox Canyon River) will be referred to as lidar M1, M2, N1, and F1, respectively, in Figs. 5–7. The CF bubbler transducer, in particular, becomes exposed to the air at water surface elevations less than ∼316 m (∼316.5 m, following its ∼0.5 m offset on 29 July 2021), with measurements from other sensors able to record lower stages. From 2019 to 2020, bank-mounted laser rangefinder M1 had the most measurements after the CF bubbler, and the two records were fit with a robust linear model (hybrid stage = $1.0647 \times$ M1 $- 20.5938$ m supply formula and $R^2 = 0.9651$), with outliers greater than ±0.25 m from the trend line removed. Beginning 16 June 2021, the additional vented Level TROLL PT provided an additional data set with higher accuracy than the bank-mounted laser rangefinder. These hourly measurements were interpolated to 15 min measurements by fitting the Level TROLL PT record with a linear model to fill gaps in the CF bubbler data (hybrid stage = $0.9515 \times$ PT $+ 15.323$ m supply formula and $R^2 = 0.9981$). The bank-mounted laser rangefinder data were no
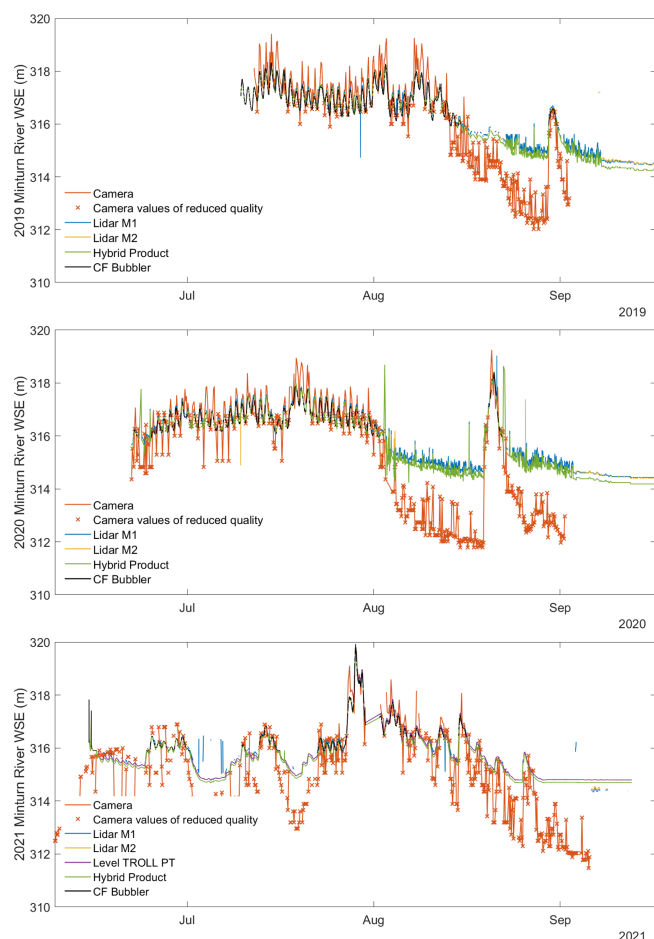
Figure 5. Hydrographs of the stage at the Minturn River were produced by two bank-mounted laser rangefinder devices (lidar M1 and lidar M2), the CF bubbler, and a hybrid product combination of the two from 2019 through 2021. In 2021, an additional vented Level TROLL PT was added at the Minturn River, providing another record of the stage. The CF bubbler record is the gold standard for accuracy but does not capture low stages, while the lower temporal resolution and more novel laser rangefinder record may have lower accuracy. A hybrid product fit a linear model to the CF bubbler and the bank-mounted laser rangefinder with fewer data gaps to produce the most complete record. Camera stage values from the lowest ~ 75 % of the riverbank, denoted with × markers, contain uncertainty due to mathematical extrapolation of the TLS bank scan below the waterline.

longer included in the hybrid stage product after the vented Level TROLL PT was installed, as the latter is more accurate. The final hybrid river stage product therefore uses the CF bubbler data when available, with gaps filled with a linear regression model based on either Level TROLL PT or laser rangefinder M1 measurements as available.

3.6 Statistical comparisons

For the quality assessment of the various experimental methods used to estimate the Minturn River stage, statistical intercomparisons were performed by calculating the R^2 and root mean square error (RMSE) values of the traditional CF bubbler vented PT with all other records (i.e., the two bank-mounted laser rangefinders, the Level TROLL PT, the time-lapse camera estimates of Goldstein et al., 2023, and the hybrid product; see Table 1). For a preliminary scientific assessment of some potential physical drivers of the Minturn River stage variations, a multivariate linear regression model was developed to assess the relationship of each AWS meteorological variable to the hybrid stage product. Correlation coefficients, p values, and scatterplots were also produced for each variable available from the meteorological station and remote sensing data sets (Fig. A2). In these correlation analyses, AWS air temperature and remotely sensed precipitation, each lagged by 0, 1, and 2 d, were considered, and net radiation was calculated as the difference between shortwave/solar downward and upward radiation. To remove high diurnal variance, all predictor variables and the hybrid river stage product were averaged to daily time steps. Any significant independent variables found were then used as predictor variables in a multivariate linear regression mode. These independent variables, albedo over the ice sheet, and air temperature, were used as predictors in a multivariate linear regression model predicting hybrid stage. Coefficients and p values were computed for each predictor.

ANOVA tests were performed on the air temperature, ice sheet albedo, precipitation, net radiation, downward radiation, and hybrid stage to assess the differences in the means between the early melt season (~ day of year (DOY) 190 to 205) for each year (2019, 2020, and 2021). The early date selection was based on visual inspection of the runoff stage records; qualitatively, the years 2019 and 2020 appear to follow similar patterns of the early high-runoff stage and the appearance of a diurnal signal, while runoff was lower and the emergence of diurnal signal was delayed in 2021. To investigate these differences, we limited our early season assessment to the period between DOY 289 (the first DOY records are available in all years) and DOY 205 (the latest onset of a pronounced diurnal signal).

4 Results

4.1 Minturn River, Inglefield Land

Proglacial river stage measurements for the Minturn River were acquired by the CF bubbler vented PT (15 min), two bank-mounted laser rangefinder units (hourly), and time-lapse cameras (Goldstein et al., 2023; 3 h) in 2019, 2020, and 2021 and by the Level TROLL vented PT (hourly) in 2021 (Fig. 5). In total, data were collected between

Table 1. Coefficients of determination (R^2) and root mean square errors (RMSEs) of different river stage sensors relative to the CF bubbler vented pressure transducer record (considered the gold standard for stage accuracy, which is ±0.003 m). Sensor pros and cons, including data completeness at 15 min, hourly, and daily time steps, are summarized.

Data set (measurement time step)	R^2 with CF bubbler	RMSE with CF bubbler (m)	Data completeness (instrument time step)	Data completeness			Pros	Cons
				15 min	Hour	Day		
CF bubbler (15 min)	n/a	n/a	44.4 %	44.4 %	49.1 %	56.6 %	Highly accurate; well-established technology	Some data intermittency; requires expert installation; contact method susceptible to river ice damage
Bank-mounted laser rangefinder (1 h)	M1: 0.809 M2: 0.739	M1: 0.256 M2: 0.251	M1: 77.1 % M2: 33.9 %	M1: 19.3 % M2: 8.5 %	M1: 77.1 % M2: 33.9 %	M1: 98.5 % M2: 62.9 %	Moderately accurate; non-contact method; simpler installation	Anomalies when Sun is low; some data intermittency
Vented Level TROLL pressure transducer (1 h)	0.996	0.050	74.5 %	18.6 %	74.5 %	96.1 %	Highly accurate; well-established technology	Requires expert installation; contact method susceptible to river ice damage
Time-lapse camera (3 h)	0.702	0.502	89.7 %	7.5 %	27.2 %	95.6 %	Non-contact method; few data gaps; simplest installation	Lower accuracy (especially in diurnal range and below TLS waterline); lower temporal resolution (3 h); gaps during some inclement weather periods
Hybrid product (15 min)	1.000*	0.000*	57.1 %	57.1 %	89.1 %	99.0 %	Most complete stage record	Derivative multisensor product with variable accuracy, depending on sensor

* Note that the hybrid stage product uses CF bubbler data when available, so these records match perfectly and are assumed to yield no error beyond the nominal sensor accuracy (±0.003 m). n/a stands for not applicable.

15 July 2019 and 12 September 2021, with prolonged winter shutdown gaps in the CF bubbler and bank-mounted laser rangefinder units from approximately 23 October 2019 to 6 June 2020 and 16 October 2020 to 14 June 2021. After quality-assurance and filtering (see Sect. 3.5), a total of 9120 (15 min) CF bubbler stage measurements, 3093 (hourly) Level TROLL PT stage measurements, 6461 (hourly) bank-mounted laser rangefinder M1 stage measurements, 3608 (hourly) bank-mounted laser rangefinder M2 measurements, and 1618 (3 h) time-lapse camera images (Goldstein et al., 2023) were acquired for the Minturn River over the three meltwater runoff seasons.

The AWS meteorological station installed at the Minturn River collected relative humidity (28 900 measurements); relative snow depth (18 707 measurements); wind direction (27 634 measurements) and speed (27 669 measurements); upward (29 212 measurements) and downward (29 214 measurements) solar radiation; air pressure (25 223 measurements); and two measures of air temperature (29 213 measurements from each) at 15 min increments. These measurements were taken from 8 July 2019 to 12 September 2021, with winter gaps from 2 September 2019 to 21 June 2020 and 15 December 2020 to 12 June 2021.

4.2 North and Fox Canyon River, Pituffik SB

For the North River at Pituffik SB, river stage measurements were recorded from 2019–2021, with two non-vented Level-logger PTs and one bank-mounted laser rangefinder, and with a Level TROLL vented PT beginning in 2021 (Fig. 6). The

longest Levelogger PT record was retrieved in June 2022 and had collected 47 692 stage measurements from 17 July 2019 to 22 May 2021, with a cold-season gap between 5 October 2019 and 1 April 2020 and no gap in the more complete Levelogger PT record during winter 2020/2021. The PT record with no gap in the winter 2020/2021 was used for this analysis. The bank-mounted laser rangefinder N1 collected 8696 stage measurements between 15 July 2019 and 25 October 2021, with winter gaps from 20 October 2019 to 16 June 2020 and 1 October 2020 to 28 April 2021. The transmitting vented Level TROLL PT operated from 7 June 2021 to 25 October 2021 and collected 2919 measurements.

For the Fox Canyon River near Pituffik SB, 8348 river stage estimates were acquired from bank-mounted laser rangefinder F1 between 15 July 2019 and 31 October 2021, with winter gaps from 29 October 2019 to 29 June 2020 and 20 October 2020 to 7 June 2021 (Fig. 7).

4.3 Sensor performances

The coefficient of determination (R^2) and root mean square error (RMSE) values computed between the gold standard CF bubbler vented pressure transducer stage record and each of the instruments installed at the Minturn River show strong correlations (Table 1). The R^2 values were 0.809, 0.739, 0.996, and 0.702, respectively, for bank-mounted laser rangefinder M1, bank-mounted laser rangefinder M2, the vented PT, and the hybrid product, respectively. Correspond-
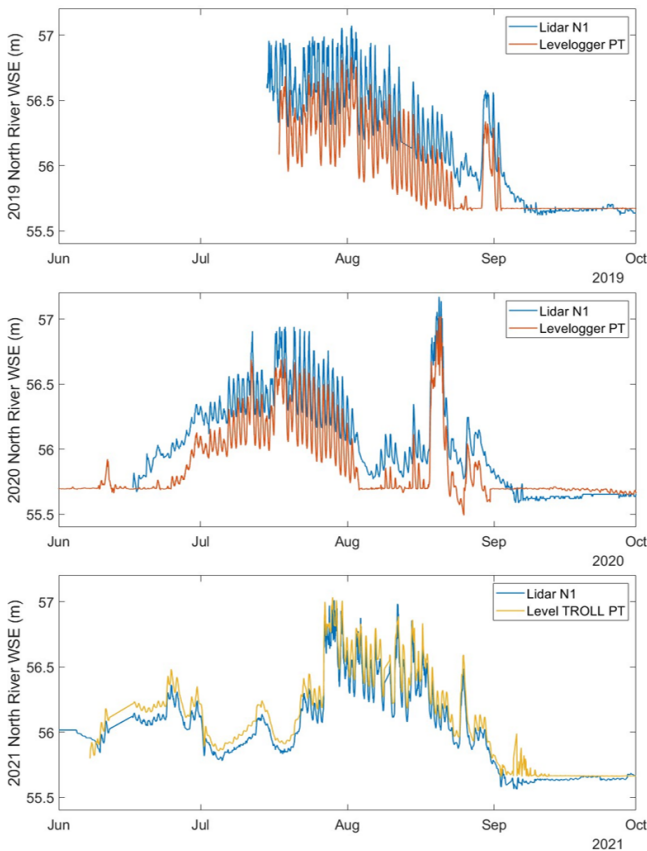
Figure 6. Records of the stage at the North River are available from a bank-mounted laser rangefinder unit (lidar N1), with an additional record of stage available from the non-vented Levelogger (2019 to 2020) and vented Level TROLL (2021) PTs.

Figure 7. Stage records from 2019 to 2021 at the Fox Canyon River are available from a bank-mounted laser rangefinder unit (lidar F1).

ing RMSE values were 0.256, 0.251, 0.050, and 0.502 m, respectively.

Each stage measurement technology (CF bubbler, Level TROLL PT, bank-mounted laser rangefinder, and camera) had different strengths and weaknesses (Table 1). The CF bubbler had the finest temporal resolution (15 min), and as the technology is considered the gold standard for river stage measurement (±0.003 m; Compact Constant Flow Bubbler, 2022), its measurements were used as the study benchmark. However, the CF bubbler installed in the Minturn River in 2019 was not submerged deeply enough to record low stages, and the instrument also missed readings at higher stages more frequently than other measurement technologies. The Level TROLL PT (RMSE $= 0.050$ m with the CF bubbler) took lower temporal resolution measurements (hourly) and was not established until 2021 but recorded lower stages and had fewer data gaps than the CF bubbler (74.5 % vs. 49.1 % at an hourly time step). The bank-mounted laser rangefinder units took hourly readings that aligned well with both the CF bubbler and Level TROLL PT measurements (RMSE with the CF bubbler is M1 $= 0.256$ and M2 $= 0.251$ m). These non-contact units were safer, easier to install, and less ex-
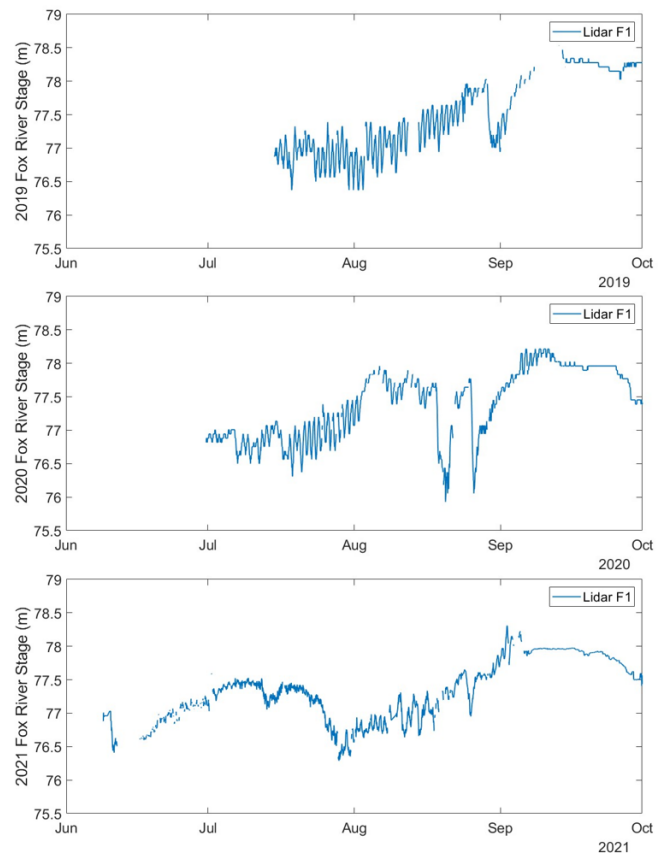
pensive than the traditional vented PTs, but solar interference occasionally caused anomalous offsets or gaps in the records (data completeness for M1 $= 77.1$ % and M2 $= 33.9$ % at an hourly time step). The time-lapse camera record matched the upward and downward movements of the CF bubbler stage well but had a substantially greater daily diurnal range, yielding the greatest RMSE of the approaches studied (RMSE $= 0.502$ m) and low quality for stage values in the lowest ~ 75 % (Goldstein et al., 2023; Fig. 5a). The cameras also only took measurements every 3 h and experienced interruptions during some adverse weather conditions (e.g., rain on the lens) of interest for stage measurement. However, the cameras were inexpensive, simple to install, experienced few data gaps (data completeness at 3 h time step $= 89.7$ %), and provided useful awareness of environmental conditions including river ice, snow, and rain.

As the instruments powered off during the cold season, data gaps were assessed during summer when all instruments were powered on and recording data. This period was taken to start at the first time step in which all instruments had acquired at least one measurement and to end on last day of stage variation (due to either ice formation or desiccation of the channel) for the winter. These dates span 15 July to

7 September 2019, 22 June to 3 September 2020, and 15 June to 29 August 2021. As laser rangefinder M2 at Minturn River did not power on until 6 July 2021 – 20 d after the all other instruments had turned on – the start of this season was taken as the first day on which all other instruments had begun recording (15 June 2021). The Level TROLL vented PT record was only available in 2021, so its statistics were computed from 2021 data only. Data completeness was calculated as the ratio of the number of measurements to the number of 15 min (CF bubbler), hourly (bank-mounted laser rangefinder and vented PT), or 3 h (camera) time periods between the start and end times each year. From these calculations, the time-lapse camera yielded the most complete data record (89.7 %), whereas laser rangefinder M2 and the CF bubbler yielded the least complete records (33.9 % and 44.4 %, respectively; Table 1).

The described differences in sensor data record completeness and accuracy encouraged the development of a hybrid product offering a more complete time series than any individual record (Fig. 5). This hybrid product, which merges stage estimates from the CF bubbler, bank-mounted laser rangefinder (2019 and 2020), and vented Level TROLL PT (2021), yields the most complete and most accurate product when compared to the CF bubbler standard (Table 1). As the CF bubbler measurements were used whenever they were available, the hybrid and bubbler record matched exactly at all time steps with bubbler records available. Overall, the hybrid product yielded the record with the fewest gaps at the 15 min (57.1 %), hourly (89.1 %), or daily (99.0 %) timescales. River stage from all instruments are presented for the Minturn River, North River, and Fox Canyon River in Figs. 5, 6, and 7, respectively.

4.4 Watershed characterization

The acquired stage records from the Minturn River, North River, and Fox Canyon River allow a preliminary assessment of runoff characteristics in the Inglefield Land and Pituffik regions. Weather conditions at the Minturn River AWS were similar between years, with air temperatures reaching highs of ~ 15 °C in July and declining thereafter, aligning with the July peak and subsequent decline in net solar radiation (Fig. 8). At all sites, river levels were high in early summer 2019 and 2020 but decreased throughout the summer and ceased flowing by September. In 2019 and 2020, the diurnal cycle of river stage was well developed by July, suggesting runoff from bare ice. This was not the case in 2021, when July diurnal cycles were suppressed at all three sites (Fig. 5). In all years, late-season rain events, as verified with camera images and decreased downward solar irradiance, triggered some sharp, late-season floods in the Minturn River (Fig. 5; 2019 and 2020), North River (Fig. 6; 2019 and 2020), and Fox Canyon River (Fig. 7; 2019).

After applying a conservative Bonferroni correction, air temperature (at all lag steps), upward/downward/net solar radiation, ice sheet/proglacial/full watershed albedo, and ice
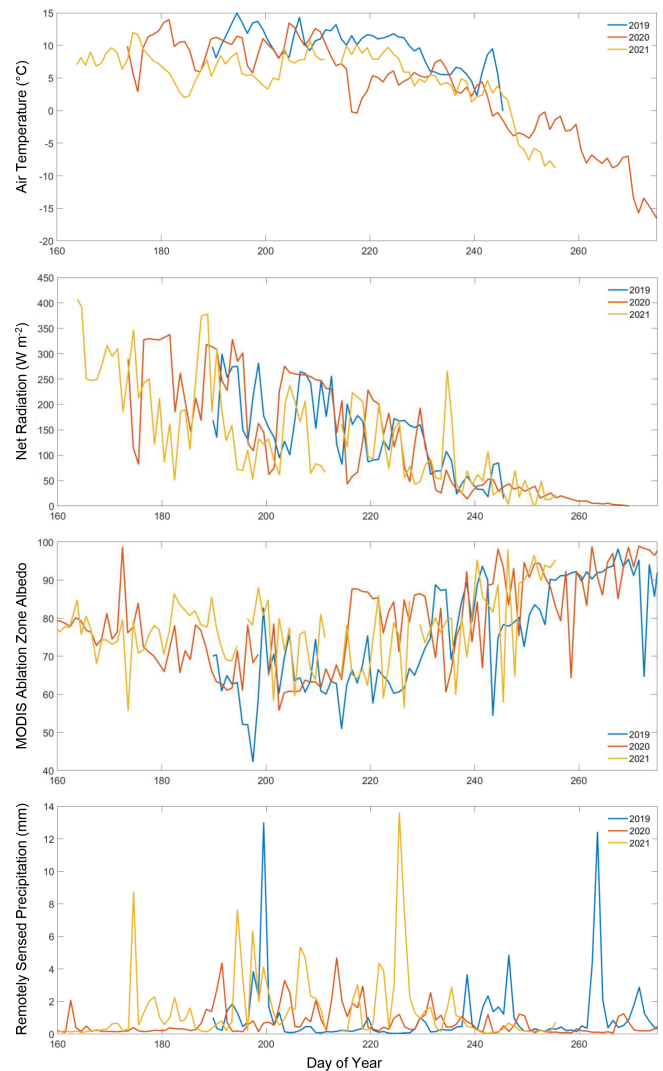

Figure 8. Daily averaged **(a)** air temperature and **(b)** net shortwave/solar radiation from the Minturn River automated weather station (AWS). Remotely sensed **(c)** ice ablation zone albedo and **(d)** precipitation from MODIS and IMERG, respectively, for DOY (day of year) 160–275.

sheet/full watershed snow cover were significantly correlated with the hybrid stage (Fig. A2). As air temperature at all lag steps (0–2 d) showed similar, strong correlation and significance values, 2 d average (lag 0–1 d) and 3 d average (lag 0–2 d) air temperature variables were introduced. The strongest predictor from each group of correlated variables was selected. This yielded 2 d average air temperature (p value $= 1.17 \times 10^{-62}$, $R^2 = 0.650$) and ablation zone albedo (p value $= 4.10 \times 10^{-71}$, $R^2 = 0.620$) that became the independent predictors included in the multivariate linear regression model for hybrid stage prediction (Fig. A2). The p values for correlation with the stage in the multivariate linear regression model were 1.38×10^{-13} and 5.73×10^{-7} for temperature and albedo, respectively. The linear model coeffi-

cients were 0.077 for 2 d average air temperature and -0.030 for ice sheet albedo. Regressions of the hybrid stage with remotely sensed precipitation at 0 to 2 d lags, air pressure, and proglacial snow cover showed no independent correlation (p values $= 8.97 \times 10^{-3}$ to 0.931; $\alpha = 2.78 \times 10^{-3}$). We conclude that air temperature and ablation zone albedo are the primary drivers of runoff stage for the Minturn watershed across seasons and years.

An early melt season analysis of variance (ANOVA) test on the yearly temperature, albedo, remotely sensed precipitation, net radiation, downward radiation, and stage data from DOY 189 (7–8 July; the first day a stage record is available in all years) to DOY 205 (23–24 July; the latest onset of a pronounced diurnal signal) indicates that significant differences were present between 2021 and 2019–2020 for the temperature, albedo, and stage. No significant differences existed between the means of remotely sensed precipitation, net radiation, or downward radiation in any years. The late June temperature and albedo were significantly cooler (11.2 and 10.1 °C in 2019 and 2020; 6.3 °C in 2021), had a more reflective ablation zone surface (0.64 and 0.65 in 2019 and 2020; 0.75 in 2021), and yielded lower river stages (317.2 and 316.9 m in 2019 and 2020; 315.7 m in 2021) in 2021 than either previous year. The p value of the difference in means is 1.17×10^{-8} for temperature, 4.70×10^{-4} for albedo, and 2.48×10^{-15} for stage. This suggests that differences in the air temperature and ablation zone albedo may have driven the differences in the early season stage between 2019–2020 and 2021.

The 2 d ($R^2 = 0.650$; p value $= 1.17 \times 10^{-62}$) and 3 d ($R^2 = 0.649$; p value $= 7.15 \times 10^{-62}$) average temperatures were more highly correlated with stage than any of the single-day measurements of air temperature (0 d lag $R^2 = 0.620$ and p value $= 1.33 \times 10^{-58}$; 1 d lag $R^2 = 0.622$ and p value $= 1.47 \times 10^{-58}$; 2 d lag $R^2 = 0.599$ and p value $= 1.11 \times 10^{-54}$). This indicates that periods of prolonged high temperature have a greater influence on stage than single-day temperatures. The similarity in the significance and correlation between the 0 and 1 d lag air temperature, with decreased significance and correlation for 2 d lag air temperature, may reflect that it takes a time period shorter than 2 d for high temperatures to produce melt and for excess meltwater runoff to be routed from across the watershed to the gauge. This conclusion is physically realistic, given the size (~ 3800 km^2, 75 % glaciated) and rough square geometry of the Minturn watershed.

The selection of multivariate regression predictors and the ANOVA analysis of the early season meteorological differences both affirm that air temperature and ice sheet albedo are primary drivers of runoff production over the Minturn watershed. Downward radiation ($R^2 = 0.311$; p value $= 1.41 \times 10^{-23}$) was a more significant driver than upward solar radiation ($R^2 = 0.161$; p value $= 6.32 \times 10^{-12}$), which could potentially reflect that decreased cloudiness leads to more meltwater runoff generation. However, albedo

over all regions (ice sheet ablation zone, proglacial zone, and full watershed) showed more significant relationships with stage, particularly for ice sheet ablation zone albedo ($R^2 = 0.620$; p value $= 4.10 \times 10^{-71}$). Given the correlation between radiation variables and albedo variables, we conclude that air temperature and ice sheet ablation zone albedo are the pre-eminent drivers of stage. This conclusion is supported by the early season ANOVA analysis, which found significant differences in ice sheet albedo and stage, but not net radiation or downward radiation, between 2019–2020 and 2021.

Precipitation was not a significant predictor of stage in the linear regression model utilizing the full 3 years of data or in the early season ANOVA analysis. This may be due to the coarse resolution (0.1° × 0.1°) of the IMERG daily accumulated precipitation data set. The limited correlation with precipitation may also be due to the infrequent and relatively small precipitation events in this high Arctic environment. Precipitation events seen in the camera imagery preceded the major floods seen in each year, suggesting that rain-on-snow events may influence the magnitude of runoff events but not be driving factors under typical (non-precipitation) conditions during the majority of the melt season.

Overall, we attribute lower proglacial river stages observed in 2021 to cooler air temperature and higher ice sheet albedo in the early part of the melt season. In the late runoff season, rainfall-induced floods occurred at all sites, as confirmed by the presence of rain in the time-lapse camera images and increased stage in the Minturn River. These findings affirm the influence of rainfall/melt events in NW Greenland, as previously demonstrated for SW Greenland by Doyle et al. (2015).

4.5 Limitations

While our installation of three proglacial river gauging stations significantly advances in situ hydrological monitoring of NW Greenland, we experienced numerous technical and logistical challenges. Submerged sensors, in particular, remain vulnerable to damage. The AWS was limited by the battery power, while the bank-mounted laser rangefinder devices were limited by the data logger date retention. The bank-mounted laser rangefinders were programmed to enter sleep mode from 31 October to 1 April, but an error in the data logger program resulted in a failure to properly retain the current date in the memory, which prevented the data logger from waking up in April 2020 and 2021. Due to COVID-19 pandemic travel bans, these issues require virtual training and emergency and service visits from Greenland-based collaborators. Installing multiple sensor technologies for river stage measurements provided increased resilience to these challenges and the opportunity to create a hybrid stage product as demonstrated here. All repairs have been completed, and all sensors are currently functional and transmitting data to the PROMICE website at this time.

5   Conclusions

We have established three new proglacial river gauging stations and one automated weather station in the NW Greenland region. The new stations provide valuable in situ observations for characterizing the timing and drivers of GrIS runoff. Following release of the stage–discharge curves established for the Minturn and North rivers, these data can be used to test SMB models used to predict surface mass loss from runoff in an understudied, rapidly changing area. Instruments installed at the Minturn River, Inglefield Land, consist of a conventional vented pressure transducer, a bubbler sensor and two experimental bank-mounted laser rangefinders to estimate the stage, two time-lapse cameras to image environmental conditions and estimate the stage, and an automated weather station to record meteorological variables (upward/-downward shortwave/solar radiation, air pressure, air temperature, relative humidity, wind speed, and wind direction). At the North River, Pituffik SB, instruments consist of one conventional vented pressure transducer, one experimental bank-mounted laser rangefinder, and two non-vented pressure transducers to measure the stage. At Fox Canyon River, near Pituffik SB, there is a bank-mounted laser rangefinder to estimate the stage. Water surface elevations at all sites are referenced to benchmarks established by this project in 2019. All instruments provided reasonably accurate, useful observations of river stage. Telemetry of these data was successful from all sites, despite the harsh environmental conditions. Redundant measurements from a suite of instruments with differing strengths and weaknesses enabled the creation of a hybrid river stage product for the Minturn River with minimal data gaps. Air temperature and ice ablation zone albedo are strongly correlated with this product, providing insight into the leading drivers of proglacial runoff in NW Greenland. All data sets are maintained and freely available through the PROMICE observational network (PROMICE, 2022).

Appendix A

Anomalous, internally consistent offsets occurred in some laser rangefinder returns between August and September of all years. In the late summer, data values were offset below the main trend line, especially between approximately 00:00 and 12:00 LT, by one of two values (Fig. A1). These two offset values (-6.00 and -9.00 m) were approximately constant across lasers at all locations, and the consistency of the offset timing suggests that the anomaly is a product of solar interference with the laser range finder. This explanation is corroborated by camera images of the Minturn River taken every 3 h, which show the strong glint on the water during the afternoon hours in the late summer. As some values recorded between 12:00 and 00:00 LT aligned with the trend line before and after the period when the anomalies were present, this subset of the data series was taken to be the true values. This data series was corrected by adding one of these two constant offset values to the falsely low values (Fig. A1).
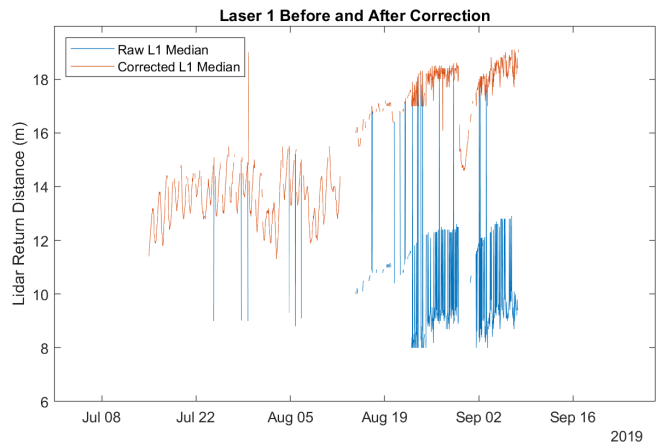

Figure A1. Two anomalous, consistent offsets were observed in the laser rangefinder returns between August and September of both 2019 and 2020, creating an upper (primary), middle, and lower trend line in the raw (blue) data. The consistency of these offsets across lasers at different locations, the presence of the offsets in only the afternoon hours of the late summer, and camera images indicating strong glint off the Minturn River during these readings suggest that solar interference with the laser range finder was the source of the anomalies. As both offsets adjusted the data by a constant value below the primary trend line, the data that were corrected by -6 or -9 m produce the corrected (red) record. Similar corrections were performed for all bank-mounted laser rangefinder records.
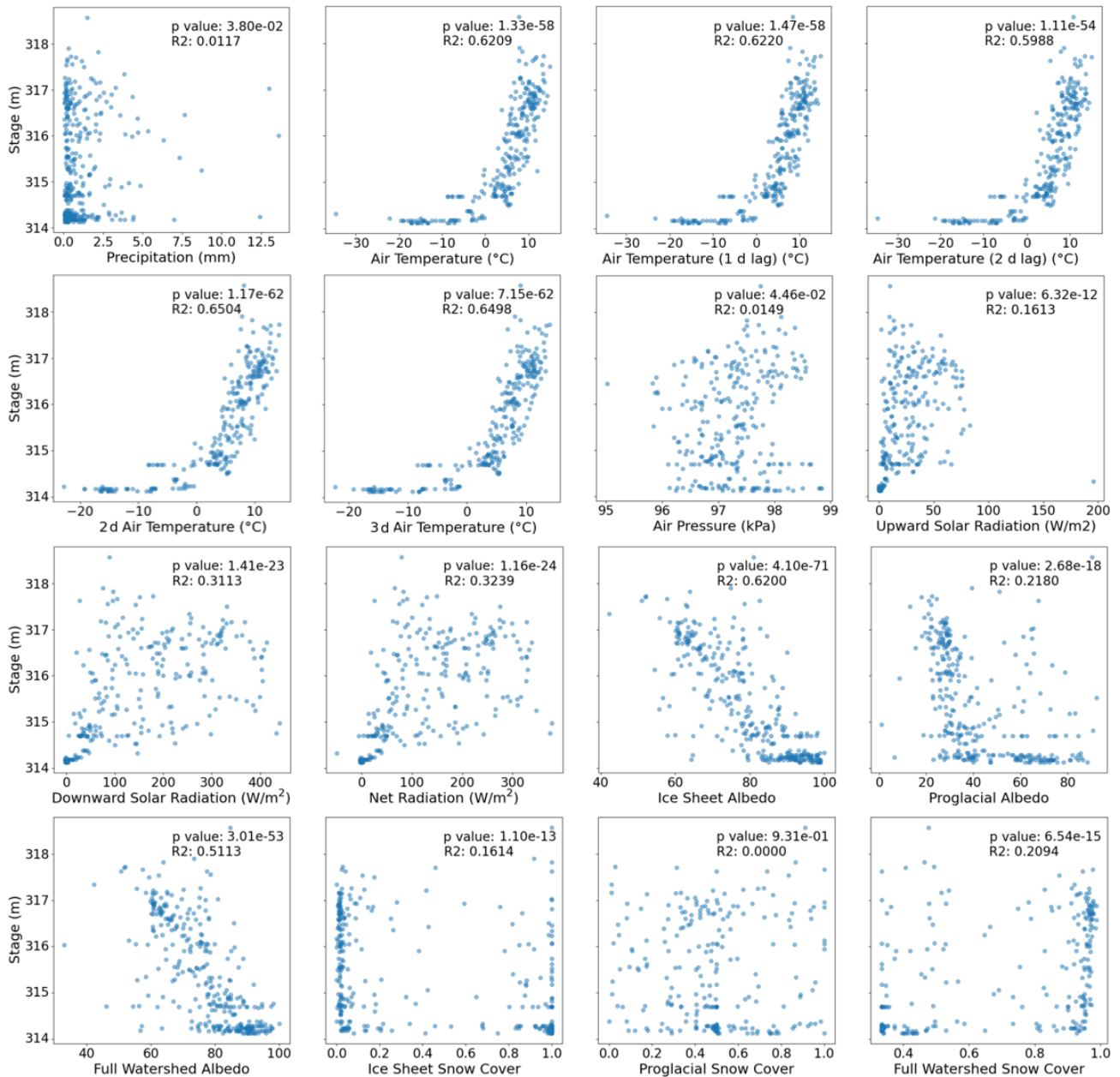
Figure A2. Scatterplots of meteorological variables with the hybrid stage. The similarity of the significance of 0 and 1 d lagged air temperature led to the inclusion of 2 d average (0 d lag and 1 d lag) and 3 d average (0, 1, and 2 d lag) air temperature. After applying a conservative Bonferroni correction to the significance threshold and selecting the variable with the strongest significance from clusters of variables, 2 d average air temperature and ice sheet (ablation zone) albedo were the significant independent predictors selected for the multivariate regression model.

References

Accubar: Accubar Barometric Pressure Sensor 5600-0120: Sutron Corporation, https://www.sutron.com/product/accubarbarometric-pressure-sensor-5600-0120/, last access: 1 November 2022.

Air Temperature: Air Temperature Sensor 5600-0020: Sutron Corporation, https://www.sutron.com/product/air-temperature-sensor-5600-0020/, last access: 1 November 2022.

Alther, G. R., Ruedisili, L. C., Stauber, H., and Kollbrunner, C. F.: Glacial melt water in Greenland: a renewable resource for the future, Int. J. Energ. Res., 5, 183–190, https://doi.org/10.1002/er.4440050207, 1981.

AT/RH: High Accuracy Sensor: Sutron Corporation, https://www.sutron.com/product/atrh-high-accuracy-sensor/, last access: 1 November 2022.

Bandini, F., Frías, M. C., Liu, J., Simkus, K., Karagkiolidou, S., and Bauer-Gottwein, P.: Challenges with Regard to Unmanned Aerial Systems (UASs) Measurement of River Surface Velocity Using Doppler Radar, Remote Sens., 14, 1277, https://doi.org/10.3390/rs14051277, 2022.

Compact Constant Flow Bubbler: Sutron Corporation, https://www.sutron.com/product/new-compact-constant-flow-cf-bubbler/, last access: 1 November 2022.

Cooper, M. G., Smith, L. C., Rennermalm, A. K., Miège, C., Pitcher, L. H., Ryan, J. C., Yang, K., and Cooley, S. W.: Meltwater storage in low-density near-surface bare ice in the Greenland ice sheet ablation zone, The Cryosphere, 12, 955–970, https://doi.org/10.5194/tc-12-955-2018, 2018.

Doyle, S. H., Hubbard, A., van de Wal, R. S. W., Box, J. E., van As, D., Scharrer, K., Meierbachtol, T. W., Smeets, P. C. J. P., Harper, J. T., Johansson, E., Mottram, R. H., Mikkelsen, A. B., Wilhelms, F., Patton, H., Christoffersen, P., and Hubbard, B.: Amplified melt and flow of the Greenland ice sheet driven by late-summer cyclonic rainfall, Nat. Geosci., 8, 647–653, https://doi.org/10.1038/ngeo2482, 2015.

Esenther, S., Smith, L. C., LeWinter, A., Pitcher, L. H, Overstreet, B. T., Kehl, A., Onclin, C., Goldstein, S., and Ryan, J. C.: New Proglacial Meteorology and River Stage Observations from Inglefield Land and Thule, NW Greenland, Zenodo [code], https://doi.org/10.5281/zenodo.8246936, 2023.

Gagliardini, O. and Werder, M. A.: Influence of increasing surface melt over decadal timescales on land-terminating Greenland-type outlet glaciers, J. Glaciol., 64, 700–710, https://doi.org/10.1017/jog.2018.59, 2018.

Goldstein, S. N., Ryan, J. C., How, P. R., Esenther, S. E., Pitcher, L. H., LeWinter, A. L., Overstreet, B. T., Kyzivat, E. D., Fayne, J. V., and Smith, L. C.: Proglacial river stage derived from georectified time-lapse camera images, Inglefield Land, Northwest Greenland, Front. Earth Sci., 11, 960363, https://doi.org//10.3389/feart.2023.960363, 2023.

GPM: GPM IMERG Final Precipitation L3 1 day 0.1° × 0.1° V06 (GPM_3IMERGDF), GES DISC, https://catalog.data.gov/dataset/gpm-imerg-final-precipitation-l3-1-day-0-1-degree-x-0-1-degree (last access: 21 September 2023), 2019.

Hofer, S., Lang, C., Amory, C., Kittel, C., Delhasse, A., Tedstone, A., and Fettweis, X.: Greater Greenland Ice Sheet contribution to global sea level rise in CMIP6, Nat. Commun., 11, 6289, https://doi.org/10.1038/s41467-020-20011-8, 2020.

Instanes, A., Kokorev, V., Janowicz, R., Bruland, O., Sand, K., and Prowse, T.: Changes to freshwater systems affecting Arctic infrastructure and natural resources, J. Geophys. Res.-Biogeo., 120, 567–585, https://doi.org/10.1002/2015JG003125, 2015.

King, M. D., Howat, I. M., Candela, S. G., Noh, M. J., Jeong, S., Noël, B. P. Y., van den Broeke, M. R., Wouters, B., and Negrete, A.: Dynamic ice loss from the Greenland Ice Sheet driven by sustained glacier retreat, Commun. Earth Environ., 1, 1–7, https://doi.org/10.1038/s43247-020-0001-2, 2020.

Kipp and Zonen: Kipp and Zonen CMP3 Pyranometer, https://www.otthydromet.com/en/p-kippzonen-cmp3-pyranometer/0338920, last access: 16 January 2023.

Li, Y., Yang, K., Gao, S., Smith, L. C., Fettweis, X., and Li, M.: Surface meltwater runoff routing through a coupled supraglacial-proglacial drainage system, Inglefield Land,

northwest Greenland, Int. J. Appl. Earth Obs., 106, 102647, https://doi.org/10.1016/j.jag.2021.102647, 2022.

Mankoff, K. D., Noël, B., Fettweis, X., Ahlstrøm, A. P., Colgan, W., Kondo, K., Langley, K., Sugiyama, S., van As, D., and Fausto, R. S.: Greenland liquid water discharge from 1958 through 2019, Earth Syst. Sci. Data, 12, 2811–2841, https://doi.org/10.5194/essd-12-2811-2020, 2020.

Mernild, S. H., Hasholt, B., and Liston, G. E.: Climatic control on river discharge simulations, Zackenberg River drainage basin, northeast Greenland, Hydrol. Process., 22, 1932–1948, https://doi.org/10.1002/hyp.6777, 2008.

Mernild, S. H., Liston, G. E., Hiemstra, C. A., Christensen, J. H., Stendel, M., and Hasholt, B.: Surface Mass Balance and Runoff Modeling Using HIRHAM4 RCM at Kangerlussuaq (Søndre Strømfjord), West Greenland, 1950–2080, J. Clim., 24, 609–623, 2011.

Mernild, S. H., Liston, G. E., van As, D., Hasholt, B., and Yde, J. C.: High-resolution ice sheet surface mass-balance and spatiotemporal runoff simulations: Kangerlussuaq, west Greenland, Arct. Antarct. Alp. Res., 50, S100008, https://doi.org/10.1080/15230430.2017.1415856, 2018.

MODIS: MODIS/Terra Snow Cover Daily L3 Global 500 m SIN Grid, Version 6, National Snow and Ice Data Center, https://nsidc.org/data/mod10a1/versions/6, last access: 16 January 2023.

Mottram, R., Simonsen, S. B., Svendsen, S. H., Barletta, V. R., Sørensen, L. S., Nagler, T., Wuite, J., Groh, A., Horwath, M., Rosier, J., Solgaard, A., Hvidberg, C. S., and Forsberg, R.: An Integrated View of Greenland Ice Sheet Mass Changes Based on Models and Satellite Observations, Remote Sens., 11, 1407, https://doi.org/10.3390/rs11121407, 2019.

Mouginot, J., Rignot, E., Bjørk, A. A., van den Broeke, M., Millan, R., Morlighem, M., Noël, B., Scheuchl, B., and Wood, M.: Forty-six years of Greenland Ice Sheet mass balance from 1972 to 2018, P. Natl. Acad. Sci. USA, 116, 9239–9244, https://doi.org/10.1073/pnas.1904242116, 2019.

Multi-Megapixel: Multi-Megapixel Hybrid IP Camera: StarDot Technologies, http://www.stardot.com/products/netcam-sc-camera (last access: 1 November 2022), 2019.

Muntjewerf, L., Petrini, M., Vizcaino, M., Ernani da Silva, C., Sellevold, R., Scherrenberg, M. D. W., Thayer-Calder, K., Bradley, S. L., Lenaerts, J. T. M., Lipscomb, W. H., and Lofverstrom, M.: Greenland Ice Sheet Contribution to 21st Century Sea Level Rise as Simulated by the Coupled CESM2.1-CISM2.1, Geophys. Res. Lett., 47, e2019GL086836, https://doi.org/10.1029/2019GL086836, 2020.

Noël, B., van Kampenhout, L., Lenaerts, J. T. M., van de Berg, W. J., and van den Broeke, M. R.: A 21st Century Warming Threshold for Sustained Greenland Ice Sheet Mass Loss, Geophys. Res. Lett., 48, e2020GL090471, https://doi.org/10.1029/2020GL090471, 2021.

Paul, J., Buytaert, W., and Sah, N.: A Technical Evaluation of Lidar-Based Measurement of River Water Levels, Water Resour. Res., 56, e2019WR026810, https://doi.org/10.1029/2019WR026810, 2020.

Ploeg, K., Seemann, F., Wild, A.-K., and Zhang, Q.: Glacio-Nival Regime Creates Complex Relationships between Discharge and Climatic Trends of Zackenberg River, Greenland (1996–2019), Climate, 9, 59, https://doi.org/10.3390/cli9040059, 2021.

PROMICE: Interactive map of automatic weather stations, The Danish Energy Agency DANCEA programme and GEUS, PROMICE [data set], https://promice.org/weather-stations/ (last access: 1 November 2022), 2023.

RIEGL: VZ-400i 3D Laser Scanning System, Riegl, USA, http://products.rieglusa.com/product/terrestrial-scanners/vz-400i-3d-laser-scanning-system# (last access: 14 September 2023), 2023.

Shepherd, A., Ivins, E., Rignot, E., Smith, B., van den Broeke, M., Velicogna, I., Whitehouse, P., Briggs, K., Joughin, I., Krinner, G., Nowicki, S., Payne, T., Scambos, T., Schlegel, N., A, G., Agosta, C., Ahlstrøm, A., Babonis, G., Barletta, V. R., Bjørk, A. A., Blazquez, A., Bonin, J., Colgan, W., Csatho, B., Cullather, R., Engdahl, M. E., Felikson, D., Fettweis, X., Forsberg, R., Hogg, A. E., Gallee, H., Gardner, A., Gilbert, L., Gourmelen, N., Groh, A., Gunter, B., Hanna, E., Harig, C., Helm, V., Horvath, A., Horwath, M., Khan, S., Kjeldsen, K. K., Konrad, H., Langen, P. L., Lecavalier, B., Loomis, B., Luthcke, S., McMillan, M., Melini, D., Mernild, S., Mohajerani, Y., Moore, P., Mottram, R., Mouginot, J., Moyano, G., Muir, A., Nagler, T., Nield, G., Nilsson, J., Noël, B., Otosaka, I., Pattle, M. E., Peltier, W. R., Pie, N., Rietbroek, R., Rott, H., Sandberg Sørensen, L., Sasgen, I., Save, H., Scheuchl, B., Schrama, E., Schröder, L., Seo, K.-W., Simonsen, S. B., Slater, T., Spada, G., Sutterley, T., Talpe, M., Tarasov, L., van de Berg, W. J., van der Wal, W., van Wessem, M., Vishwakarma, B. D., Wiese, D., Wilton, D., Wagner, T., Wouters, B., Wuite, J., and The IMBIE Team: Mass balance of the Greenland Ice Sheet from 1992 to 2018, Nature, 579, 233–239, https://doi.org/10.1038/s41586-019-1855-2, 2020.

Smith, L. C., Chu, V. W., Yang, K., Gleason, C. J., Pitcher, L. H., Rennermalm, A. K., Legleiter, C. J., Behar, A. E., Overstreet, B. T., Moustafa, S. E., Tedesco, M., Forster, R. R., LeWinter, A. L., Finnegan, D. C., Sheng, Y., and Balog, J.: Efficient meltwater drainage through supraglacial streams and rivers on the southwest Greenland ice sheet, P. Natl. Acad. Sci. USA, 112, 1001–1006, https://doi.org/10.1073/pnas.1413024112, 2015.

Smith, L. C., Yang, K., Pitcher, L. H., Overstreet, B. T., Chu, V. W., Rennermalm, Å. K., Ryan, J. C., Cooper, M. G., Gleason, C. J., Tedesco, M., Jeyaratnam, J., van As, D., van den Broeke, M. R., van de Berg, W. J., Noël, B., Langen, P. L., Cullather, R. I., Zhao, B., Willis, M. J., Hubbard, A., Box, J. E., Jenner, B. A., and Behar, A. E.: Direct measurements of meltwater runoff on the Greenland ice sheet surface, P. Natl. Acad. Sci. USA, 114, E10622–E10631, https://doi.org/10.1073/pnas.1707743114, 2017.

Smith, L. C., Andrews, L. C., Pitcher, L. H., Overstreet, B. T., Rennermalm, Å. K., Cooper, M. G., Cooley, S. W., Ryan, J. C., Miège, C., Kershner, C., and Simpson, C. E.: Supraglacial River Forcing of Subglacial Water Storage and Diurnal Ice Sheet Motion, Geophys. Res. Lett., 48, e2020GL091418, https://doi.org/10.1029/2020GL091418, 2021.

Trusel, L. D., Das, S. B., Osman, M. B., Evans, M. J., Smith, B. E., Fettweis, X., McConnell, J. R., Noël, B. P. Y., and van den Broeke, M. R.: Nonlinear rise in Greenland runoff in response to post-industrial Arctic warming, Nature, 564, 104–108, https://doi.org/10.1038/s41586-018-0752-4, 2018.

van Dalum, C. T., van de Berg, W. J., and van den Broeke, M. R.: Impact of updated radiative transfer scheme in snow and ice in RACMO2.3p3 on the surface mass and energy budget

of the Greenland ice sheet, The Cryosphere, 15, 1823–1844, https://doi.org/10.5194/tc-15-1823-2021, 2021.

Wind Speed and Direction Sensor: Sutron Corporation, https://www.sutron.com/product/wind-speed-direction-sensor/, last access: 1 November 2022.

Yang, K. and Smith, L. C.: Internally drained catchments dominate supraglacial hydrology of the southwest Greenland Ice Sheet, J. Geophys. Res.-Earth, 121, 1891–1910, https://doi.org/10.1002/2016JF003927, 2016.

Yang, K., Smith, L. C., Sole, A., Livingstone, S. J., Cheng, X., Chen, Z., and Manchun, L.: Supraglacial rivers on the northwest Greenland Ice Sheet, Devon Ice Cap, and Barnes Ice Cap mapped using Sentinel-2 imagery, Int. J. Appl. Earth Obs., 78, 1–13, https://doi.org/10.1016/j.jag.2019.01.008, 2019.

Yang, K., Smith, L. C., Cooper, M. G., Pitcher, L. H., van As, D., Lu, Y., and Li, M.: Seasonal evolution of supraglacial lakes and rivers on the southwest Greenland Ice Sheet, J. Glaciol., 67, 592–602, https://doi.org/10.1017/jog.2021.10, 2021.